Title
Li2S nano spheres anchored to single-layered graphene as a high-performance cathode material for lithium/sulfur cells

Authors
Sun, Dan
Hwa, Yoon
Shen, Yue
et al.

Publication Date
2016-08-01

DOI
10.1016/j.nanoen.2016.05.033

Nano Energy 26 (2016) 524–532

Contents lists available at ScienceDirect

Nano Energy

journal homepage: www.elsevier.com/locate/nanoen

Li_2S nano spheres anchored to single-layered graphene as a high-performance cathode material for lithium/sulfur cells

Dan Sun [a,b,c], Yoon Hwa [a,b], Yue Shen [c], Yunhui Huang [c], Elton J. Cairns [a,b,*]

[a] Department of Chemical and Biomolecular Engineering, University of California, Berkeley, CA 94720, United States
[b] Energy Technologies Area, Lawrence Berkeley National Laboratory, Berkeley, CA 94720, United States
[c] State Key Laboratory of Material Processing and Die & Mold Technology, School of Materials Science and Engineering, Huazhong University of Science and Technology (HUST), Wuhan, Hubei 430074, China

ARTICLE INFO

Article history:
Received 27 March 2016
Received in revised form
13 May 2016
Accepted 20 May 2016
Available online 24 May 2016

Keywords:
Lithium batteries
Energy storage
Sulfur
Lithium sulfide
Graphene
Carbon coating

ABSTRACT

Fully lithiated lithium sulfide (Li_2S) has become a promising cathode material for Li/S cells due to its high theoretic capacity (1166 mA h g^{-1}) and specific energy (2600 W h kg^{-1}). However, low utilization of sulfur and poor rate capability still hinder the practical application of Li/S cells. In this paper, a carbon coated Li_2S/graphene composite (Li_2S/G@C) was developed by incorporating Li_2S nano spheres with single-layered graphene and further forming a durable protective carbon layer on the surface of the Li_2S particles using a facile CVD method. The high rate capability and remarkable cycle life of the Li_2S/G@C cathode were demonstrated, which was mainly attributed to the unique structure of the Li_2S/G@C that can significantly improve not only the electrical conductivity, but also the mechanical stability of the sulfur cathode.

1. Introduction

With increasing numbers of vehicles and growing demands on fossil energy in the past several decades, the coupled resource depletion and critical environmental pollution have raised an urgent need for alternatives to fossil fuels and combustion engines. The utilization of intermittent renewable energy such as wind and solar power, have attracted tremendous attention and provided an ecologically friendly and sustainable solution to meet the exponentially increasing demand for energy. Thus, high specific energy rechargeable battery systems of low-cost for energy storage are essential. Among the many candidates, the lithium-ion battery (LIB) is considered as "state-of-the-art" and has been used for portable devices and electric vehicles [1–7]. However, the traditional LIB seems to be insufficient for practical application in emerging markets due to the limited specific energy of the cell, which indicates that remarkable developments are necessary for applications such as electric vehicles [8–10].

Lithium/sulfur(Li/S) cells have been investigated since the 1960s and have drawn tremendous attention in recent years due to its rather high theoretical capacity of 1675 mA h g^{-1} ($S_8 + 16Li \rightarrow 8Li_2S$) and specific energy of 2600 W h kg^{-1}, indicating a superior energy storage capability. Furthermore, sulfur, which is ubiquitous in nature, is environmentally benign and low-cost. [4,8–15] Li/S cells have become one of the most promising rechargeable cell systems, showing great potential in meeting the rigorous needs for electrical vehicles and grid-scale stationary storage. Despite their advantages, Li/S cells still are affected by some intrinsic drawbacks. The dissolution of lithium polysulfides into organic liquid electrolytes and its "shuttle effect" together with mechanical degradation of the sulfur cathode (caused by severe volume change of sulfur particles (up to 80%) during cycling) limits the Li/S cell lifetime, meanwhile, the electrically insulating nature of sulfur and Li_2S causes sluggish reaction kinetics, resulting in low electrochemical utilization of the active material and poor rate capability [16,17]. As a result of efforts to address these issues significant improvements have been made in recent years by coupling sulfur to various carbon materials (e.g., graphene, graphene oxide (GO), and carbon fibers), polymers (e.g., polyethylene glycol (PEG), polypyrrole (PPY), polyacrylonitrile (PAN)) and transition metal oxides with novel hierarchical and core-shell configurations to overcome the drawbacks of the sulfur cathode [4,18–29]. In addition, another difficulty of the Li/S cells is the use of a metallic lithium anode, which is associated with dendrite formation on the surface of the Li metal anode caused by the inhomogeneous current distribution during cycling, leading to serious safety hazards and cell shorting [30–32].

* Corresponding author at: Department of Chemical and Biomolecular Engineering, University of California, Berkeley, CA 94720, United States.
E-mail address: ejcairns@lbl.gov (E.J. Cairns).

http://dx.doi.org/10.1016/j.nanoen.2016.05.033
2211-2855/

Fully lithiated lithium sulfide (Li_2S) with a theoretical specific capacity of 1169 mA h g^{-1} Li_2S has become a more desirable cathode material for the Li/S cell due to its capability of pairing with a lithium-free anode such as silicon and some tin compounds which can obviate the safety concerns of the lithium metal anode when using sulfur [10,33–41]. Li_2S particles, as the end discharge product of the Li/S cell, shrink during charging and generate empty space to accommodate the volume expansion of sulfur particles during lithiation (discharge), thus the mechanical failure of the cathode can be alleviated, resulting in improved cycle life for the Li/S cell. Moreover, the higher melting point of Li_2S (1372 °C) [42] enables modifications under high temperature treatment conditions such as chemical vapor deposition (CVD) that can provide a uniform and stable carbon coating on the particle surface [35,36,43]. Sharing the same reaction mechanisms, Li_2S cathodes inevitably encounter the same problems as for sulfur cathodes such as the dissolution of polysulfides into most liquid electrolytes, and its "shuttle effect" which can induce low utilization of active material, low coulombic efficiency and severe degradation of the cycle life. Meanwhile the low electronic and ionic conductivity of Li_2S also cause low sulfur utilization and poor rate capability of the sulfur cathode [10,44]. To address the above-mentioned problems, many approaches have emerged to improve the electrochemical performance of the Li_2S cathode, for example employing Li_2S nanoparticles, and encapsulating Li_2S with carbon, [1,10,35] conductive polymers or transition metal disulfides [37,45]. In addition, some functional carbon materials such as carbon nanofibers, graphene and GO are also used to enhance the electrical conductivity of the Li_2S cathode material [36,46–49].

Herein, an especially efficient structure of single-layered graphene bonded to carbon coated Li_2S nano spheres (Li_2S/G@C) is demonstrated and used as a cathode material for the Li/S cell, showing high specific capacity and excellent cyclability. Single-layered graphene was used as a conductive host for Li_2S nano sphere deposition and all the Li_2S/graphene composites were further treated with the CVD method to form a very stable and electrically conductive carbon shell on the surface of the Li_2S nano spheres which can not only provide individual void spaces to accommodate the volume change caused by transition between Li_2S and elemental S, but also act as a protective shield against polysulfide dissolution during cycling. We found that the use of graphene flakes can greatly affect the morphology of the Li_2S/graphene composite and CVD results. With the optimized procedure, a Li_2S/G@C composite with uniformly distributed ultra-fine carbon coated Li_2S nano spheres (~100 nm) on both sides of single-layered graphene was synthesized. As the highly conductive substrate, graphene can facilitate the electron transport in the cathode material. In addition, the sluggish lithium ion diffusion through the insulating sulfur (or Li_2S) can be accommodated by the nano-sized Li_2S particles. The Li_2S/G@C cathode exhibited excellent rate capability and long cycle life, high reversible initial capacities of 993 mA h g^{-1} of Li_2S (1420 mA h g^{-1} of S), 773 mA h g^{-1} of Li_2S (1105 mA h g^{-1} of S) and 743 mA h g^{-1} of Li_2S (1062 mA h g^{-1} of S) can be obtained at 0.5 C, 1 C, and 2 C rates respectively (1 C = 1166 mA h g^{-1}, Li_2S). After 1000 cycles at a rate of 2 C for both charge and discharge, a capacity of 314 mA h g^{-1} of Li_2S (451 mA h g^{-1} of S) still retained, which is significantly higher than that of a new Li ion cell.

2. Experimental section

2.1. Material synthesis

Due to the high sensitivity of Li_2S to moisture, all the synthesis procedures and furnace tube assembly/disassembly were conducted in an argon-filled glove box with a moisture content below 0.1 ppm and oxygen level below 0.6 ppm. The Li_2S/G@C Nano-composites were prepared as follows: Different amount of graphene (3 mg, 5 mg, 8 mg, 10 mg) were firstly dispersed in 4.2 mL 1.0 M lithium triethylborohydride in tetrahydrofuran (1 M LiEt3BH in THF, Sigma-Aldrich) under ultra-sonication for 10 min. Then 3 mL toluene containing 2 mmol sulfur (Alfa Aesar, Sulfur powder ~325 mesh, 99.5%) was added into the prepared solution and stirred at room temperature. After 5 min, the mixture was heated to 90 °C under continuous stirring to precipitate lithium sulfide nano-spheres. The Li_2S/G composite was washed with THF and hexane via centrifugation twice. After being dried inside of a glove box overnight the collected sample was heat-treated at 500 °C for 30 min. To estimate the weight percentage of pure Li_2S inside of the Li_2S/G composite, a certain amount of Li_2S/G powder after heat treatment was weighted and washed with deionized water via filtration for several times until the pH of the filtered solution reached 7, then the powder was dried under vacuum at 50 °C overnight and weighted again. The Li_2S reacted with water during the process, so comparing the weight difference between Li_2S/G and the washed powder would provide the weight ratio between pristine Li_2S and Li_2S/G composite (90–97 wt%). To obtain carbon coated Li_2S spheres the Li_2S/G composite was heated to 450 °C and maintained at 450 °C for 30 min using argon gas and acetylene (carbon precursor) with a flow rate of 100 sccm (standard cubic centimeters per minute) and 10 sccm, respectively. The amount of carbon deposited can be calculated by weighting the composite before and after the CVD process (8–19 wt%). To increase the stability as well as the electronic conductivity of the carbon shell, the as obtained Li_2S/G@C composite was further heated at 750 °C for about 30 min.

2.2. Electrochemical measurement

The cathodes were prepared by grinding a mixture containing active material, carbon black (super P) and polyvinylpyrrolidone (PVP; Mw ~1300 K) (pure Li_2S: C: PVP = 60:30:10, by weight) for 10 min, then dispersing the mixture in N-methyl-2-pyrrolidinone (NMP) to make slurry with a concentration of 250 mg mL^{-1} and stirring for 4 h, coating the slurry onto an aluminum foil and evaporating the solvent under 50 °C inside of a glove box and drying overnight. The electrode area is 1.13 cm^2, the mass loading of Li_2S and S in the electrodes are 1.1–1.4 mg/cm^2 and 0.76–0.97 mg/cm^2 respectively. 0.7 M LiTFSI (Lithium Bis(Trifluoromethanesulfonyl)Imide) in PYR_{14}TFSI (N-methyl-N-butylpyrrolidinium bis(trifluoromethane sulfonyl)imide)/DOL(dioxolane)/DME(Dimethoxyethane) (2:1:1, by volume) containing 0.5 M $LiNO_3$ (lithium nitrate) was used as electrolyte. CR2325 coin cells were assembled in an argon filled glove box. The cell consisted of the electrodes fabricated, lithium metal foil anode (99.98%, Cyprus Foote Mineral) and porous polypropylene separator (Celgard 2400). Electrochemical performance of the cells was evaluated with a battery cycler (Arbin BT2000) between 1.7 V and 2.8 V after being charged to 4 V for the first charge.

2.3. Characterization

The structure of the samples was investigated with an X-ray diffractometer (XRD, Bruker AXS D8 Discover GADDS micro-diffractometer) with a Co Kα radiation source. An air-free holder was used to provide an inert atmosphere for the Li_2S samples during the test. The morphology and particle size of the samples were examined using a field emission scanning electron microscope (FESEM, JEOL JSM-7500F) with elemental mapping using energy-dispersive X-ray spectroscopy (EDS, Oxford). High resolution transmission electron microscopy images were collected using a 200 kV FEI monochromated F20 UT Tecnai instrument.

As for the polysulfide dissolution test, 1 mg of commercial Li_2S, #3-Li_2S/G@C, #5-Li_2S/G@C and #8-Li_2S/G@C were each added into a 1.5 mL THF/toluene mixture (1:1, by volume) containing 7 mg sulfur.

3. Results and discussion

The synthesis process for the Li_2S/G@C is illustrated in Fig. 1a. Considering the stacking nature of graphene, different amounts of commercial single-layered graphene (Fig. S1) (3 mg, 5 mg, 8 mg and 10 mg) were first dispersed in a solution of lithium triethylborohydride ($LiEt_3BH$) in tetra-hydrofuran (THF) via ultra-sonication to form a homogeneous graphene/$LiEt_3BH$ mixture. Sulfur powder was dissolved in toluene and then added to the as-prepared graphene-$LiEt_3BH$ mixture solution [50]. Li_2S is synthesized on the basis of the following chemical reaction:

$$S + 2LiEt_3BH \rightarrow Li_2S + 2Et_3BH + H_2 \quad (1)$$

The same amount of Li_2S in all Li_2S/G composites was obtained by controlling the amount of sulfur used, and Li_2S spheres were uniformly deposited on the surface of the graphene sheets after the evaporation of the solvent. A facile CVD method was conducted at 450 °C for 30 min using acetylene gas as a carbon source to form a uniform carbon protection layer on the surface of the Li_2S spheres. More detailed information about the synthesis process of the Li_2S/G@C composite is available in the supporting information. The X-ray diffraction (XRD) patterns of prepared samples are displayed in Fig. 1b, all XRD peaks observed in the XRD patterns of the prepared Li_2S/G@C composites can be indexed by the cubic structure of Li_2S (Fm3m, PDF#65-2981), indicating that pure Li_2S was successfully fabricated in all samples. XRD Peaks attributed to LiOH were caused by the reaction of Li_2S with moisture during testing.

The mass fraction of the graphene, the protective carbon layer formed via CVD and the Li_2S of the prepared Li_2S/G@C composites depending on the different amounts of graphene during synthesis are individually displayed in Table 1. In order to investigate the microstructure of each sample, scanning electron microscopy (SEM) characterization was carried out and the results are shown in Fig. 2. It can be expected that the amount of graphene in the precursor solution has a dramatic influence on the morphology of the samples, because the total surface area of single-layered graphene which provides the sites for heterogeneous nucleation of Li_2S depends on the amount of graphene added. Due to the lower nucleation barrier Li_2S will be preferentially nucleated on the surface of the graphene. With a smaller amount of graphene, independent Li_2S spheres will form due to a lack of surface available for Li_2S formation. It was confirmed by the SEM images of sample #3-Li_2S/G@C (Fig. 2a and b) that was prepared with the smallest amount of graphene, the structure of #3-Li_2S/G@C was composed of both graphene sheets covered with ultra-fine Li_2S particles and the independent Li_2S nano spheres with a uniform size of 500 nm. When the amount of graphene increased, the independent Li_2S nano spheres disappeared and the spherical Li_2S on the graphene was only observed in the #5 and #8-Li_2S/G@C composites (Fig. 2c–f), although the #5-Li_2S/G@C composite still showed agglomeration of Li_2S nano particles in some parts, which might cause a non-uniform particle size distribution and less effective carbon coating. Compared to samples #3 and #5, #8-Li_2S/G@C composite showed the most promising morphology in which the Li_2S spheres were uniformly distributed on single-layered graphene sheets with a particle size of 50–100 nm, which is beneficial for the enhancement of electrical conductivity attributed to the efficient electronic pathway through a conformal carbon coating and the graphene sheet, together with a short pathway for Li ions through the reduced Li_2S particle size. In the #10-Li_2S/G@C composite (Fig. S2), some exposed graphene surface remained due to the excess

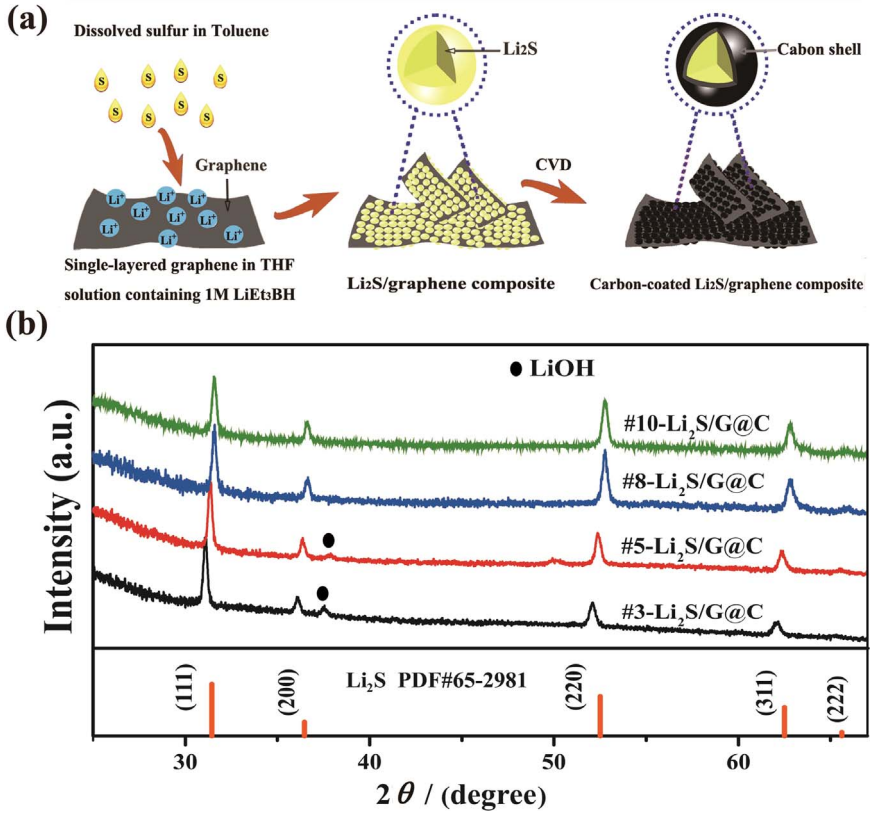

Fig. 1. (a) Fabrication process of the Li_2S/G@C composite. (b) X-ray diffraction patterns of the synthesized Li_2S/G@C composites. Cobalt was used as XRD source.

Table 1
Detailed information about the Li_2S/G@C composites.

Carbon-coated Li_2S/graphene sample	Amount of graphene added	Mass fraction of graphene	Mass fraction of carbon layer with CVD	Mass fraction of Li_2S
#10-Li_2S/G@C	10 mg	7.9 wt%	19 wt%	73.1 wt%
#8-Li_2S/G@C	8 mg	6.9 wt%	13.1 wt%	80 wt%
#5-Li_2S/G@C	5 mg	5.2 wt%	11 wt%	83.8 wt%
#3-Li_2S/G@C	3 mg	5.1 wt%	8 wt%	86.9 wt%

amount of graphene and that provides sites for the growth of carbon nanofibers (CNFs) during the CVD process, which is probably due to some catalyst residues left in the graphene. The growth of CNFs causes difficulty in controlling both the Li_2S particle size distribution and the amount of carbon coating, so the #10-Li_2S/G@C will not be discussed in this paper.

To further explore the differences among these composites, galvanostatic charge–discharge tests of coin cells with #3,5 and 8-Li_2S/G@C as cathode materials were performed to compare the electrochemical performances of the different cathodes. In order to obtain high capacity in cells, it is very important to increase the conductivity of electrode and use an optimized cell composition. In our work, the role of the ionic liquid in the electrolyte is to palliate the high mobility of polysufides and to improve the capacity and rate capability of the cells [51,52]. $LiNO_3$ is believed to be an effective additive in the electrolyte that not only helps the electrochemical oxidation of Li_2S, but also prevents polysulfides from contacting the Li anode by generating a protective film on the Li metal anode. Because $LiNO_3$ may be irreversibly reduced on the cathode at potentials lower than 1.6 V (vs. Li/Li^+), the discharge cutoff voltage here was set at 1.7 V to avoid capacity fade due to reduction of the nitrate [53,54]. In addition, a large overpotential was always observed during the initial charging process that was associated with the initial formation of polysulfide. In order to overcome the high energy barrier all the cells were charged to 4.0 V at a relatively low C rate of 0.05 C during the first cycle [10].

The rate capabilities of all the Li_2S/G@C electrodes are shown in Fig. 3a, even though good capacities can be obtained with #3, #5 and #8-Li_2S/G@C cathodes at 0.2 C, the specific capacity of the #3 and #5-Li_2S/G@C composite cathodes dramatically decreased as the discharge rate increased. This capacity loss with increased rates is directly associated with the conductivity of the cathodes [55]. In contrast, the #8-Li_2S/G@C cathode showed the best rate capability and delivered specific capacities of 1029.8 mA h g^{-1} of Li_2S (1472 mA h g^{-1} of S), 831.6 mA h g^{-1} of Li_2S (1189 mA/ h g^{-1} of S), 769 mA h g^{-1} of Li_2S (1099 mA h g^{-1} of S) and 672.8 mA h g^{-1} of Li_2S (962 mA h g^{-1} of S) at charge/discharge rates of 0.2 C, 0.5 C, 1.0 C and 2.0 C (1.0 C=1166 mA h g^{-1} Li_2S), respectively. More importantly, for all the cathodes highly reversible specific capacities recovered to more than 1100 mA h g^{-1} of S when the C rate was switched back to 0.2 C after 60 cycles, indicating good rate capability and good recovery of the cathodes.

Fig. 3b–d shows representative voltage profiles of each cathode at different C rates. For consideration of stability, we chose the voltage profile at the second cycle of each different C rate. Two discharge plateaus in the range of 2.4–2.1 V and 2.1–1.7 V, respectively, were observed, which are related to the stepwise reactions between Li_2S and solid S_8 molecules [8]. The second discharge plateau was more sensitive to the discharge C rate [55], consequently, all the cathodes revealed decreased utilization of sulfur and increased overpotentials as the discharge C-rate increased. Both the #8 and #5-Li_2S/G@C could undergo reversible redox reactions at higher C rates, however, #8-Li_2S/G@C showed the lowest charge and discharge overpotentials at each C rate and exhibited a stable plateau even at the high C rate of 2 C, demonstrating a remarkable electronic conductivity and the lowest energy loss associated with charge/discharge overpotentials owing to the combination of the highly conductive graphene substrate and the carbon coating.

The cycling performance of all the cathodes charged and discharged at 0.5 C is presented in Fig. 3e, and initial capacities of 993 mA h g^{-1} of Li_2S (1420 mA h g^{-1} of S), 960.7 mA h g^{-1} of Li_2S (1374.5 mA h g^{-1} of S) and 871 mA h g^{-1} of Li_2S (1245 mA h g^{-1} of S) were obtained with the #8, #5 and #3-Li_2S/G@C cathodes,

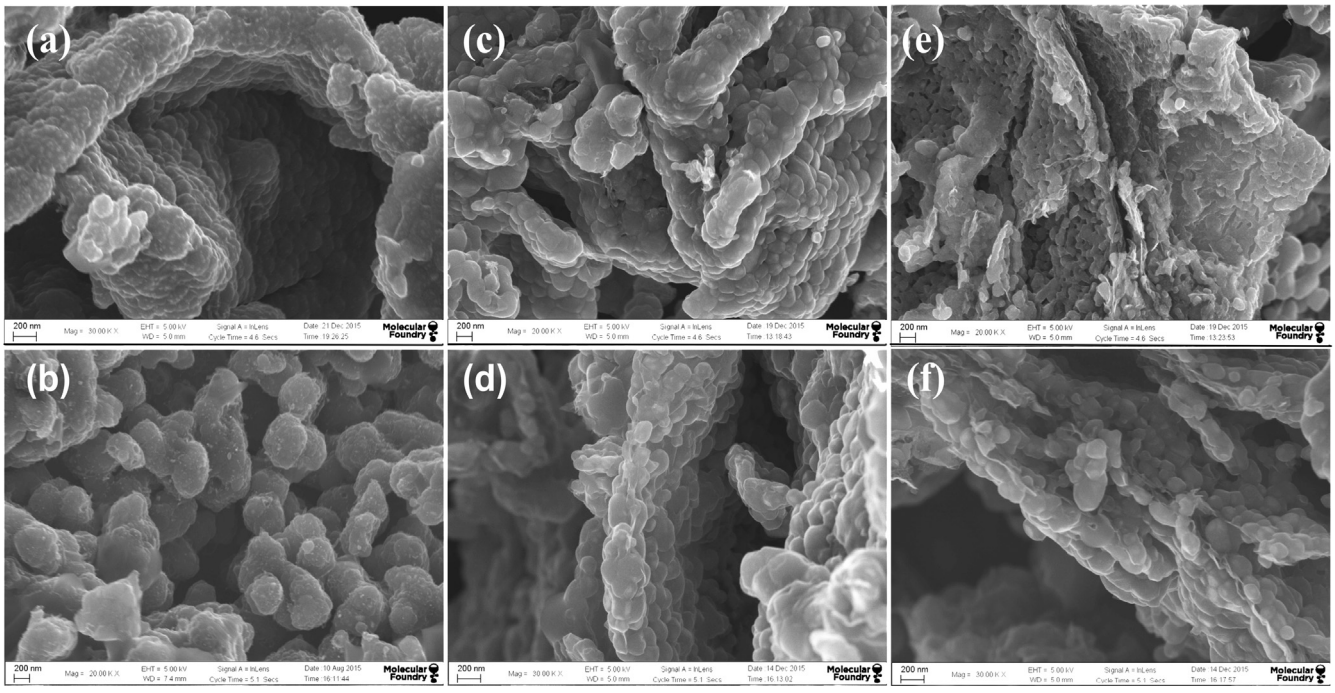

Fig. 2. SEM images of the (a, b) #3-Li_2S/G@C; (c, d) #5-Li_2S/G@C; and (e, f) #8-Li_2S/G@C composites. (e) TEM image of hollow carbon nano-sphere including GO in its structure obtained by removal of Li_2S from the Li_2S/GO@C nano-sphere.

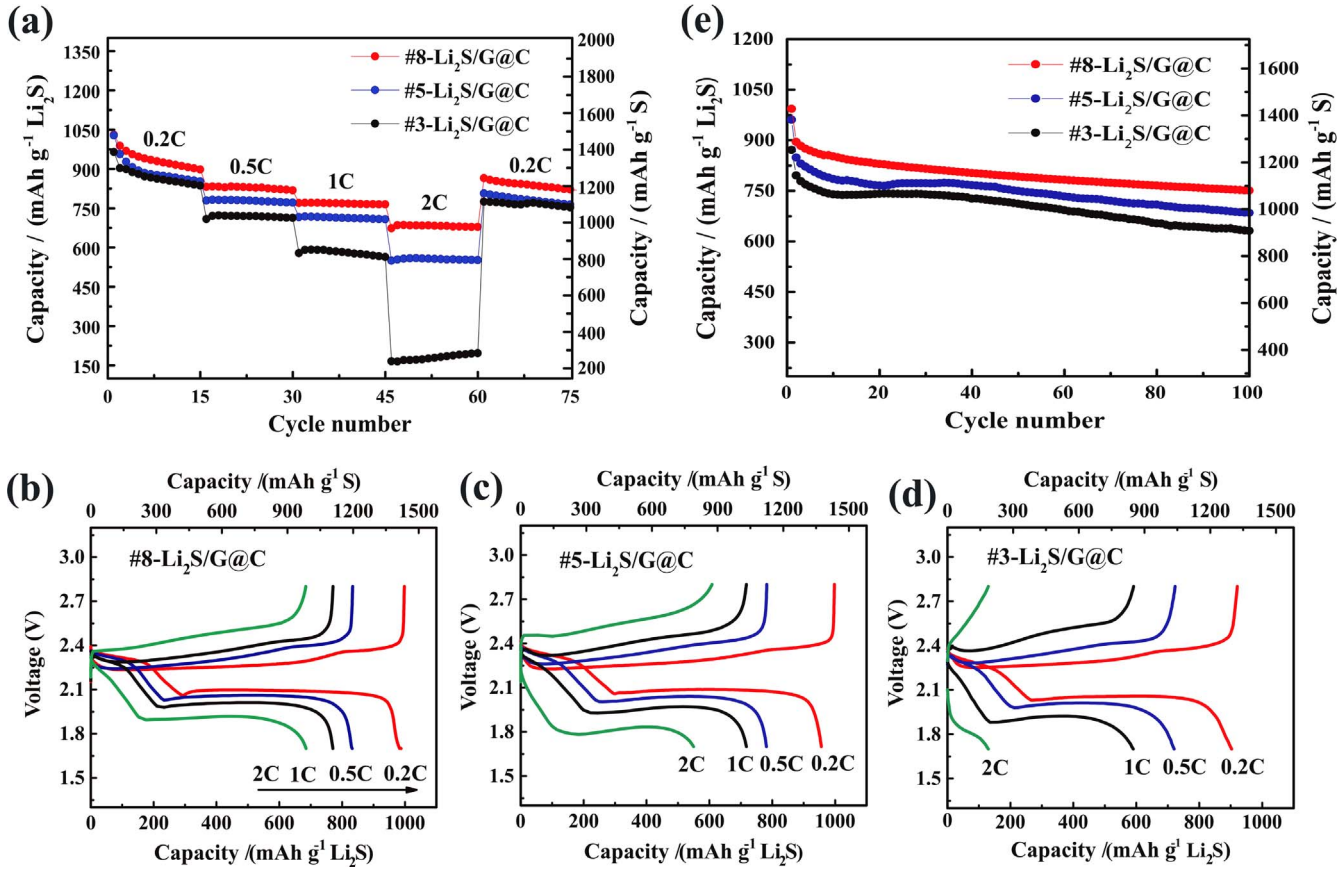

Fig. 3. Electrochemical characterization of the #3, 5 and 8-Li_2S/G@C composites. (a) Rate performance of the Li_2S/G@C cathodes at different discharge C rates from 0.2 C to 2.0 C. Charge and discharge profiles for the second cycle of (b) the #8-Li_2S/G@C, (c) the #5- Li_2S/G@C and (d) the #3-Li_2S/G@C cathodes at various C-rates. (e) Cycling performance of the #3, 5 and 8-Li_2S/G@C cathodes at 0.5 C discharge. The cathode composition was, pure Li_2S: C: PVP=60:30:10, by weight. The mass loading of Li_2S in the electrodes were 1.1–1.3 mg /cm^2 (corresponding to 0.76–0.9 mg/cm^2 of S).

respectively. A similar small capacity fade (~100 mA h g^{-1} of Li_2S) was measured for all cathodes at the second cycle, which is probably due to a minor loss of active material caused by imperfect protection of the carbon layer during the first cycle. The highest discharge specific capacity of up to 751 mA h g^{-1} of Li_2S (1074 mA h g^{-1} of S) was still retained with #8-Li_2S/G@C cathode after 100 cycles. Interestingly, the first charge plateau of all cathodes (Fig. S8) displayed relatively low overpotentials compared to the results reported by most researchers, and the overpotentials gradually decreased as the amount of graphene increased, which might indicate higher electronic conductivity, good lithium ion diffusivity in the Li_2S and faster charge transfer at the Li_2S surface in the #8-Li_2S/G@C composite [10,36].

The long-term cycling stability was conducted at a high charge and discharge C rate of 2.0 C for 1000 cycles and the results are shown in Fig. 4. As shown in Fig. 4e, the #8-Li_2S/G@C cathode exhibited both the highest discharge specific capacity and cycling capability for 1000 cycles. A specific capacity of 315 mA h g^{-1} of Li_2S (450 mA h g^{-1} of S) was obtained after prolonged cycling period of 1000 cycles with a Coulombic efficiency of over 99.5% during cycling. Abrupt specific capacity increase with decrease of Coulombic efficiency occurred within the first 100 cycles, which may be related to the following: (i) the deformation of the carbon shell and Li_2S redistribution during cycling, when the cells were charged at 2.0 C, a small part of active material may not be involved the reaction in the first several cycles but might be activated after the cathode structure reaches a stable configuration [56]; (ii) polysulfides generated as a result of imperfect carbon coating or failure of the protective layer will shuttle back to the cathode and be oxidized to higher-order polysulfides, leading to a slight capacity increase; (iii) the special single-layered graphene structure may undergo minor structural changes during early cycles at high C rates.

The voltage profiles of the 10th, 200th, 500th and 1000th cycles at 2.0 C for each cathode are displayed in Fig. 4a–c. As tested under the same C rate, the disparities placed in the durability of plateaus, serious capacity loss and overpotential increases occurred after 200 cycles for the #5-Li_2S/G@C cathode (Fig. 4b), which might because of the polysulfide dissolution. Meanwhile, the critical "shuttle effect" during cycling at 2 C could be one possibility to lead to the poor cycling performance of the #3-Li_2S/G@C cathode (Fig. 4c). On the contrary, excellent cycling capability was obtained by the #8-Li_2S/G@C cathode (Fig. 4a), which exhibited steady discharge plateaus around 2 V during discharge even after 1000 cycles, and more importantly, the increase of overpotentials during cycling turned out be very small. The SEM images of the #8-Li_2S/G@C electrode before and after 1000 cycles are also presented in Fig. S9, despite minor deformation of the carbon shells, the microstructure of spherical nano particles uniformly distributed on single-layered graphene sheet still remained, indicating high stability of the electrode structure.

Polysulfide dissolution tests were conducted to detect the degree of protection provided by and the stability of the protective carbon shell formed during the CVD process. Polysulfide will be produced by the reaction of Li_2S in the cathode material with the dissolved sulfur in the test solution, which causes the color change of the test solution from clear to dark orange. So the color of the test solution should change quickly if the carbon protection layer is not sufficient to isolate the Li_2S core form the solvent. As displayed in Fig. 5a, bare Li_2S powder exhibited a dark orange color

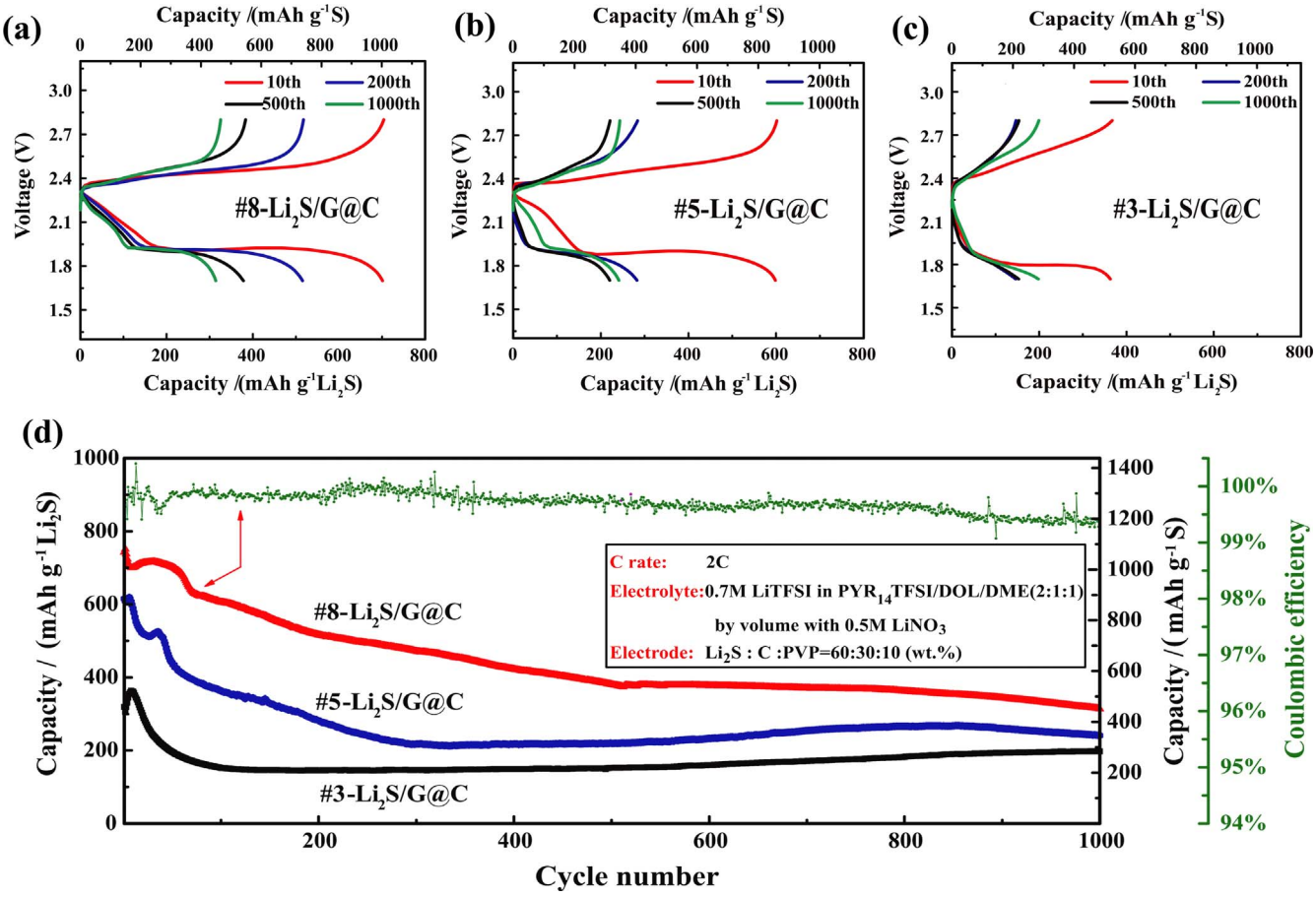

Fig. 4. Charge and discharge voltage profiles of the (a) #8-Li_2S/G@C composite, (b) #5-Li_2S/G@C composite and (c) #3-Li_2S/G@C composite cathodes. (d) Comparison of the long-term cycling performance of the #3, #5 and #8-Li_2S/G@C composite cathodes at 2.0 C and coulombic efficiency of #8-Li_2S/G@C electrode for 1000 cycles. The cathode composition was, pure Li_2S: C: PVP=60:30:10, by weight. The mass loadings of Li_2S in the cathodes were 1.1–1.3 mg/cm^2 (corresponding to 0.76–0.9 mg/cm^2 of S).

after 10 days which indicates that a reaction occurred between Li_2S and the dissolved sulfur. The test solution colors of the #3-Li_2S/G@C and the #5-Li_2S/G@C composites also turned to light orange after 10 days and became darker in the following days and it is noticeable that the carbon layer of the #5-Li_2S/G@C seems to provide better protection against the loss of Li_2S. The test solution of #8-Li_2S/G@C composite remained clear even after 20 days and only showed a slight color change after 30 days, indicating that a substantially protective carbon layer was formed on the Li_2S nanoparticles after CVD and successfully suppresses the penetration of solvent into the inner core. The #8-Li_2S/G@C composite sample was washed with deionized water via ultra-sonication for 5 min, and the dried sample was then tested by transmission electron microscope (TEM, Fig. S7). In Fig. S7, the carbon shells can be observed, validating the structural stability of as-formed carbon protection. Since the CVD deposit is essentially the thermolysis product of acetylene (C_2H_2) which can be strongly affected by the condition of the surface, fast deposition of carbon occurred at surfaces with high activity. When using the same amount of carbon source, materials with smaller particle size and less agglomeration were likely to exhibit more conformal and stable carbon coatings. The CVD results obtained from polysulfide dissolution tests were in good agreement with the morphologies observed by SEM and the positive effect of a durable carbon layer on the electrochemical performance by suppressing polysulfide dissolution and enhancing the electronic conductivity of the #8-Li_2S/G@C composite.

As discussed above, the introduction of graphene can significantly affect the morphology and the electrochemical performance of as-synthesized Li_2S/G@C composites, so high capacity together with high rate capability and cycling stability of cathode material can be achieved by employing an optimal amount of graphene and generating a durable protective carbon layer on the Li_2S particles via the CVD process. Since the #8-Li_2S/G@C composite showed the best electrochemical performance among all the samples, it would be instructive to investigate further the electrochemical and structural features of the composite. The cycling performance test results of the #8-Li_2S/G@C composite cathode presented in Fig. 5b shows an initial discharge specific capacity of 993 mA h g^{-1} of Li_2S (1420 mA h g^{-1} of S), 773 mA h g^{-1} of Li_2S (1105 mA h g^{-1} of S) and 743 mA h g^{-1} of Li_2S (1062 mA h g^{-1}of S) at a charge/discharge rate of 0.5 C, 1.0 C and 2.0 C, respectively. After 100 cycles, the cells still could deliver high specific capacities of 750 mA h g^{-1} of Li_2S (1072 mA h g^{-1} of S), 712 mA h g^{-1} of Li_2S (1018 mA h g^{-1} of S) and 606 mA h g^{-1} of Li_2S (866 mA h g^{-1} of S) at 0.5 C, 1.0 C and 2.0 C, respectively. It is notable that the high specific capacity retention of 92% after 100 cycles was obtained at the 1.0 C rate. The voltage profiles at the 10th cycle at each C rate (Fig. 5c) exhibited similar curves with the voltage profiles shown in Fig. 3b and indicates the high electrical conductivity and structural stability of the #8-Li_2S/G@C composite.

To further investigate the electrochemical behavior of the #8-Li_2S/G@C composite cathode, cyclic voltammetry (CV) was conducted for 5 cycles at a slow scan rate of 0.025 mV/s and the results are displayed in Fig. 5d. The potential was swept from the OCV to 4.0 V followed by a sweeping between 1.7 V and 2.8 V. Two anodic peaks related to the energy barrier for the conversion of pristine Li_2S to sulfur during the first charge process were present

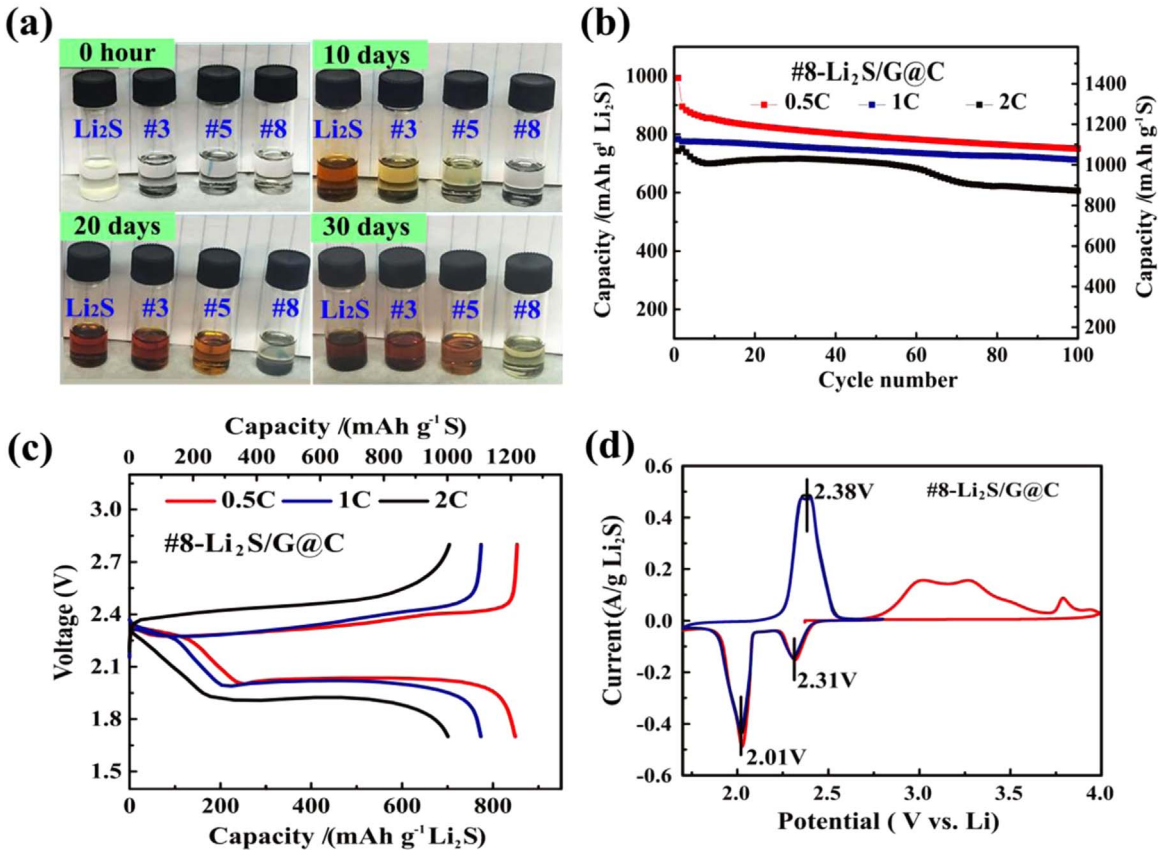

Fig. 5. (a)Polysulfide dissolution test results of commercial Li_2S and as synthesized #3, #5 and #8-Li_2S/G@C composite. (b) Comparison of cycling stability of the #8-Li_2S/G@C cathode at C rates of 0.5 C, 1.0 C and 2.0 C. (c) Voltage profiles of the 10th cycle at C rates of 0.5 C, 1 C and 2 C. (d) Cyclic voltammograms of the #8-Li_2S/G@C cathode at a scan rate of 0.025 mV/s. The cathode composition was, pure Li_2S: C: PVP=60:30:10, by weight. The mass loading of Li_2S in the cathodes were 1.1–1.4 mg/cm^2 (corresponding to 0.76–0.97 mg/cm^2 of S).

at a relatively low voltage of less than 3.5 V compared to the results shown in previous reports, which might indicate the positive effects of the small particle size of Li_2S with less agglomeration of the #8-Li_2S/G@C composite [35]. The redox peaks centered at 2.34 V and the sharp peak at 2.05 V during discharge can be attributed to the stepwise reaction from the S_8 molecule to long-chain polysulfide Intermediates and further to the final product Li_2S (or Li_2S_2). The anodic peak that appeared at 2.32 V with a shoulder is associated with the conversion of Li_2S to S_8. The small voltage shifting between cathodic and anodic peaks reflects a low overvoltage of the cell and indicates a high reversibility of the cell reaction. The striking features displayed in the CV curves revealed good capacity retention and cycling stability of the #8-Li_2S/G@C composite cathode which was enabled by the reduced particle size of Li_2S and the conformal carbon coating on the Li_2S surface.

To further demonstrate the structure of the #8-Li_2S/G@C composite, SEM observation with energy dispersive X-ray spectroscopy (EDS) was conducted (Fig. S10), which confirmed the homogeneous distribution of sulfur (corresponding to Li_2S based on the XRD pattern) and carbon (graphene and carbon coating layer) in the #8-Li_2S/G@C composite. The oxygen signal might be contributed by LiOH which formed during sample transfer to the

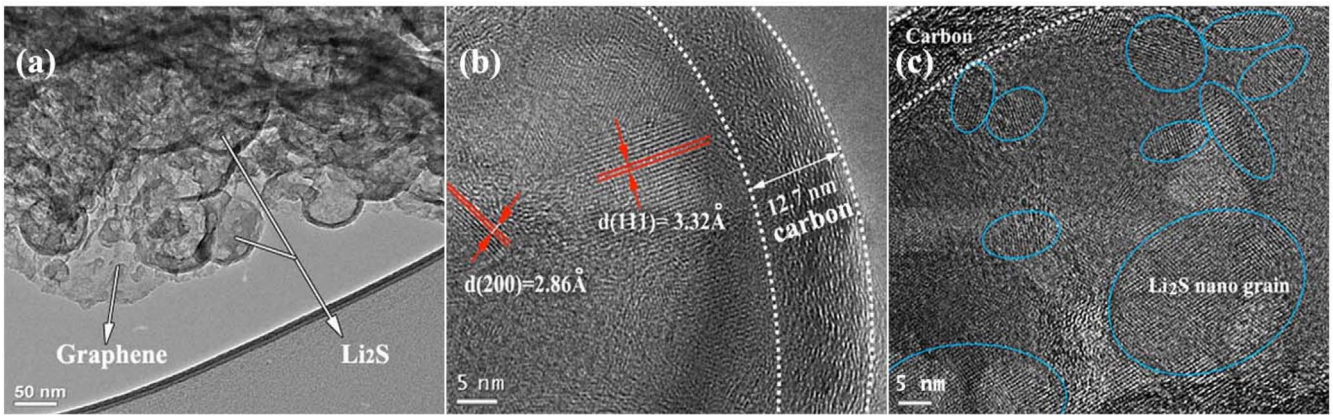

Fig. 6. TEM characterization of the #8-Li_2S/G@C composite: (a) low magnification TEM image of the #8-Li_2S/G@C composite. (b) High resolution TEM image of the #8-Li_2S/G@C composite which shows the thickness of the carbon layer and the interplanar spacing within the Li_2S particles which are assigned to the (111) and (200) planes of Li_2S; (c) high resolution TEM image of the #8-Li_2S/G@C composite which shows the nano-grains of Li_2S.

SEM chamber. In order to elucidate the core-shell structure formed during CVD and the microstructure of the #8-Li_2S/G@C composite, transmission electron microscopy (TEM) was conducted (Fig. 6a–c). As shown in the low magnification TEM image of the #8-Li_2S/G@C (Fig. 6a), Li_2S nano spheres with a size of ~100 nm were well encapsulated in a uniform carbon layer and bonded to the graphene sheets. Since the sample was exposed to the moisture in air during transfer of the sample into the TEM chamber, bright holes inside of the carbon shell could be observed due to the sulfur loss caused by the reaction between Li_2S and moisture that generates H_2S gas. A conformal turbostatic carbon layer was detected by high resolution TEM with thickness that ranged from 12 nm to 14 nm, as shown in Fig. 6b. Distinct lattices with d-spacings of 0.332 nm and 0.286 nm that correspond to the (111) and (200) planes of Li_2S, respectively, were observed, demonstrating the crystalline Li_2S inside the carbon layer. More importantly, in some well-preserved particles, as displayed in Fig. 6c, the poly-crystalline structure of Li_2S with very small nano-grains was observed, which could dramatically shorten the lithium diffusion distance and enhance the diffusion rate of Li ions inside Li_2S particle by allowing Li ions to transfer through these nano grain boundaries. It can be suggested that the unique nano-structure of Li_2S contributed to the excellent rate performance of the #8-Li_2S/G@C composite cathode.

4. Conclusion

In summary, we synthesized Li_2S/G@C nanocomposites by combining graphene with Li_2S nano spheres and further forming a durable protective carbon layer on the surface of the Li_2S particles using a facile CVD method. By comparing and investigating the influence of the amount of graphene on both physical structure and electrochemical properties of Li_2S/G@C, a promising structure of single-layered graphene bonded to conformal carbon-coated Li_2S nano spheres was developed. The success of this Li_2S/G@C electrode affording high rate capability and cycling stability with a good capacity retention was ascribed to the following: (i) Uniform nano-sized particle distribution of Li_2S on graphene resulting in a very conformal carbon coating after CVD which assisted in preventing Li_2S from contact with electrolyte and suppressing the polysulfide dissolution and capacity decay; (ii) Improved electronic conductivity resulting from both a highly conductive graphene substrate and a conformal carbon layer formed via CVD effectively facilitated fast transport of electrons in the electrodes; (iii) Reduced lithium diffusion limitations, attributed to the reduced particle size and specific crystal structure of the Li_2S nano spheres providing high Li ion transport rates which together with enhanced electronic conductivity can significantly improve the rate performance and cycling stability of the electrode; (iv) Robust structure of the Li_2S/G@C also contributed to the stability of the electrode under long-term cycling.

Acknowledgment

We thank Tevye Kuykendall and the LBNL Molecular Foundry at the Lawrence Berkeley National Laboratory for supporting the X-ray diffractometer and scanning electron microscopy. Work at the Molecular Foundry was supported by the Office of Science Office of Basic Energy Sciences, of the U.S. Department of Energy under Contract no. DE-AC02–05CH11231. We appreciate the experimental help from Junchao Zheng. Thanks also go to Xiangyun Song and Zhiyuan Zeng for help with the transmission electron microscope at the National Center for Electron Microscopy and the Material Science Division, respectively. Dan Sun acknowledges a fellowship from the China Scholarship Council (CSC) to perform this work at UC Berkeley and LBNL.

Appendix A. Supplementary material

Supplementary data associated with this article can be found in the online version at http://dx.doi.org/10.1016/j.nanoen.2016.05.033.

References

[1] Y.Z. Fu, Y.S. Su, A. Manthiram, Adv. Energy Mater. 4 (2014).
[2] A. Manthiram, S.H. Chung, C.X. Zu, Adv. Mater. 27 (2015) 1980–2006.
[3] J.M. Tarascon, M. Armand, Nature 414 (2001) 359–367.
[4] X.L. Ji, K.T. Lee, L.F. Nazar, Nat. Mater. 8 (2009) 500–506.
[5] J.B. Goodenough, K.S. Park, J. Am. Chem. Soc. 135 (2013) 1167–1176.
[6] J.B. Goodenough, Energy Environ. Sci. 7 (2014) 14–18.
[7] L. Chen, Y.Z. Liu, N. Detz-Rago, L.L. Shaw, Nanoscale 7 (2015) 18071–18080.
[8] P.G. Bruce, S.A. Freunberger, L.J. Hardwick, J.M. Tarascon, Nat. Mater. 11 (2012) 19–29.
[9] Q.F. Zhang, Y.P. Wang, Z.W. Seh, Z.H. Fu, R.F. Zhang, Y. Cui, Nano Lett. 15 (2015) 3780–3786.
[10] K.P. Cai, M.K. Song, E.J. Cairns, Y.G. Zhang, Nano Lett. 12 (2012) 6474–6479.
[11] E.J. Cairns, H. Shimotake, Science 164 (1969) 1347–1355.
[12] T. Kobayashi, Y. Imade, D. Shishihara, K. Homma, M. Nagao, R. Watanabe, T. Yokoi, A. Yamada, R. Kanno, T. Tatsumi, J. Power Sources 182 (2008) 621–625.
[13] L.W. Ji, M.M. Rao, S. Aloni, L. Wang, E.J. Cairns, Y.G. Zhang, Energy Environ. Sci. 4 (2011) 5053–5059.
[14] J.T. Lee, Y.Y. Zhao, S. Thieme, H. Kim, M. Oschatz, L. Borchardt, A. Magasinski, W.I. Cho, S. Kaskel, G. Yushin, Adv. Mater. 25 (2013) 4573–4579.
[15] Z. Li, J.T. Zhang, X.W. Lou, Angew. Chem. Int. Ed. 54 (2015) 12886–12890.
[16] J. Nelson, S. Misra, Y. Yang, A. Jackson, Y.J. Liu, H.L. Wang, H.J. Dai, J.C. Andrews, Y. Cui, M.F. Toney, J. Am. Chem. Soc. 134 (2012) 6337–6343.
[17] Y.V. Mikhaylik, J.R. Akridge, J. Electrochem. Soc. 151 (2004) A1969–A1976.
[18] T.Z. Zhuang, J.Q. Huang, H.J. Peng, L.Y. He, X.B. Cheng, C.M. Chen, Q. Zhang, Small 12 (2016) 381–389.
[19] Z.L. Ma, S. Dou, A.L. Shen, L. Tao, L.M. Dai, S.Y. Wang, Angew. Chem. Int. Ed. 54 (2015) 1888–1892.
[20] Z. Wang, Y. Dong, H. Li, Z. Zhao, H.B. Wu, C. Hao, S. Liu, J. Qiu, X.W. Lou, Nat. Commun. 5 (2014) 5002.
[21] H.L. Wang, Y. Yang, Y.Y. Liang, J.T. Robinson, Y.G. Li, A. Jackson, Y. Cui, H.J. Dai, Nano Lett. 11 (2011) 2644–2647.
[22] Y. Yang, G.H. Yu, J.J. Cha, H. Wu, M. Vosgueritchian, Y. Yao, Z.A. Bao, Y. Cui, ACS Nano 5 (2011) 9187–9193.
[23] G.C. Wang, Y.Q. Lai, Z.A. Zhang, J. Li, Z.Y. Zhang, J. Mater. Chem. A 3 (2015) 7139–7144.
[24] Y.R. Li, L.X. Yuan, Z. Li, Y.Z. Qi, C. Wu, J. Liu, Y.H. Huang, RSC Adv. 5 (2015) 44160–44164.
[25] N. Brun, K. Sakaushi, L.H. Yu, L. Giebeler, J. Eckert, M.M. Titirici, Phys. Chem. Chem. Phys. 15 (2013) 6080–6087.
[26] H. Hu, H.Y. Cheng, Z.F. Liu, G.J. Li, Q.C. Zhu, Y. Yu, Nano Lett. 15 (2015) 5116–5123.
[27] M.K. Song, Y.G. Zhang, E.J. Cairns, Nano Lett. 13 (2013) 5891–5899.
[28] Z. Li, J.T. Zhang, Y.M. Chen, J. Li, X.W. Lou, Nat. Commun. 6 (2015).
[29] J.T. Zhang, H. Hu, Z. Li, X.W. Lou, Angew. Chem. Int. Ed. 55 (2016) 3982–3986.
[30] X.B. Cheng, H.J. Peng, J.Q. Huang, F. Wei, Q. Zhang, Small 10 (2014) 4257–4263.
[31] M. Rosso, C. Brissot, A. Teyssot, M. Dolle, L. Sannier, J.M. Tarascon, R. Bouchetc, S. Lascaud, Electrochim. Acta 51 (2006) 5334–5340.
[32] W. Xu, J.L. Wang, F. Ding, X.L. Chen, E. Nasybutin, Y.H. Zhang, J.G. Zhang, Energy Environ. Sci. 7 (2014) 513–537.
[33] J. Hassoun, Y.K. Sun, B. Scrosati, J. Power Sources 196 (2011) 343–348.
[34] J. Liu, H. Nara, T. Yokoshima, T. Momma, T. Osaka, J. Power Sources 273 (2015) 1136–1141.
[35] C.Y. Nan, Z. Lin, H.G. Liao, M.K. Song, Y.D. Li, E.J. Cairns, J. Am. Chem. Soc. 136 (2014) 4659–4663.
[36] Y. Hwa, J. Zhao, E.J. Cairns, Nano Lett. 15 (2015) 3479–3486.
[37] Z.W. Seh, J.H. Yu, W. Li, P.C. Hsu, H. Wang, Y. Sun, H. Yao, Q. Zhang, Y. Cui, Nat. Commun. 5 (2014) 5017.
[38] Y. Yang, M.T. McDowell, A. Jackson, J.J. Cha, S.S. Hong, Y. Cui, Nano Lett. 10 (2010) 1486–1491.
[39] Y. Yang, G.Y. Zheng, S. Misra, J. Nelson, M.F. Toney, Y. Gui, J. Am. Chem. Soc. 134 (2012) 15387–15394.
[40] A. Hayashi, R. Ohtsubo, T. Ohtomo, F. Mizuno, M. Tatsumisago, J. Power Sources 183 (2008) 422–426.
[41] C.X. Zu, M. Klein, A. Manthiram, J. Phys. Chem. Lett. 5 (2014) 3986–3991.
[42] P.T. Cunningham, S.A. Johnson, E.J. Cairns, J. Electrochem. Soc. 119 (1972) 1448–1450.
[43] F. Wu, J.T. Lee, E. Zhao, B. Zhang, G. Yushin, ACS Nano 10 (2016) 1333–1340.
[44] F.Y. Fan, W.C. Carter, Y.M. Chiang, Adv. Mater. 27 (2015) 5203–5209.
[45] Z.W. Seh, H.T. Wang, P.C. Hsu, Q.F. Zhang, W.Y. Li, G.Y. Zheng, H.B. Yao, Y. Cui,

Energy Environ. Sci. 7 (2014) 672–676.
[46] C. Wang, X.S. Wang, Y. Yang, A. Kushima, J.T. Chen, Y.H. Huang, J. Li, Nano Lett. 15 (2015) 1796–1802.
[47] F.X. Wu, J.T. Lee, A. Magasinski, H. Kim, G. Yushin, Part. Part. Syst. Charact. 31 (2014) 639–644.
[48] F.X. Wu, A. Magasinski, G. Yushin, J. Mater. Chem. A 2 (2014) 6064–6070.
[49] Z. Lin, C.Y. Nan, Y.F. Ye, J.H. Guo, J.F. Zhu, E.J. Cairns, Nano Energy 9 (2014) 408–416.
[50] J.A. Gladysz, V.K. Wong, B.S. Jick, Tetrahedron 35 (1979) 2329–2335.
[51] J.M. Zheng, M. Gu, H.H. Chen, P. Meduri, M.H. Engelhard, J.G. Zhang, J. Liu, J. Xiao, J. Mater. Chem. A 1 (2013) 8464–8470.
[52] J.W. Park, K. Ueno, N. Tachikawa, K. Dokko, M. Watanabe, J. Phys. Chem. C 117 (2013) 20531–20541.
[53] H.S. Kim, T.G. Jeong, N.S. Choi, Y.T. Kim, Ionics 19 (2013) 1795–1802.
[54] S.S. Zhang, Electrochim. Acta 70 (2012) 344–348.
[55] S.-E. Cheon, K.-S. Ko, J.-H. Cho, S.-W. Kim, E.-Y. Chin, H.-T. Kim, J. Electrochem. Soc. 150 (2003) A796.
[56] G. Zheng, Q. Zhang, J.J. Cha, Y. Yang, W. Li, Z.W. Seh, Y. Cui, Nano Lett. 13 (2013) 1265–1270.

Dan Sun is a Ph.D. candidate in Huazhong University of Science and Technology and now a visiting researcher under the supervision of Prof. Elton J. Cairns at the University of California, Berkeley. Her research interests focus mainly on the developing cathode material for electrochemical energy storage and conversion, including lithium-air batteries and lithium-sulfur batteries.

Dr. Yoon Hwa received his Ph.D. in Materials Science and Engineering at the Seoul National University in 2013. After his Ph.D., he has worked with Prof. Elton J. Cairns at Lawrence Berkeley National Laboratory as a postdoctoral fellow. His research interests focus on developing advanced electrochemical energy storage and conversion systems including lithium ion cells and lithium/sulfur cells.

Prof. Yue Shen received his B. S. degree in chemistry and Ph.D. degree in material science from Peking University in 2011. He is now an associate professor in Huazhong University of Science and Technology. His research interest includes functional nanomaterials and lithium-air batteries.

Prof. Yun-Hui Huang received his B. S., M. S. and Ph.D. from Peking University. In 2000, he worked as a postdoctoral researcher in Peking University. From 2002 to 2004, he worked as an associate professor in Fudan University and a JSPS fellow at Tokyo Institute of Technology, Japan. He then worked with Prof. John B. Goodenough in the University of Texas at Austin for more than three years. In 2008, he became a chair professor of materials science in Huazhong University of Science and Technology. His research group works on batteries of energy storage and conversion.

Prof. Elton J. Cairns University of California, Berkeley, and Lawrence Berkeley National Laboratory Elton J. Cairns received his B. S. in Chemistry and B. S. in Chemical Engineering at the Michigan Technological University, and his Ph.D. at the University of California, Berkeley. He currently serves as Professor of the Graduate School in Chemical Engineering, University of California, Berkeley, and Faculty Senior Scientist, Lawrence Berkeley National Laboratory. Dr. Cairns has published in the areas of electrochemical kinetics, batteries, fuel cells, molten salts, liquid metals, thermodynamics, surface chemistry, catalysis, and transport phenomena.